








Magnetization dynamics of granular heat-assisted magnetic recording media by means of a multiscale model

A. Meo ^{1,*} W. Pantasri,¹ W. Daeng-am ¹ S. E. Rannala ² S. I. Ruta ² R. W. Chantrell,² P. Chureemart ¹ and J. Chureemart ^{1,†}

¹*Department of Physics, Mahasarakham University, Mahasarakham 44150, Thailand*

²*Department of Physics, University of York, York YO10 5DD, United Kingdom*

 (Received 28 April 2020; revised 16 October 2020; accepted 22 October 2020; published 12 November 2020)

Heat-assisted magnetic recording (HAMR) technology represents the most promising candidate to replace the current perpendicular recording paradigm to achieve higher storage densities. To better understand HAMR dynamics in granular media we need to describe accurately the magnetization dynamics up to temperatures close to the Curie point. To this end we propose a multiscale approach based on the Landau-Lifshitz-Bloch (LLB) equation of motion parametrized using atomistic calculations. The LLB formalism describes the magnetization dynamics at finite temperature and allows us to efficiently simulate large system sizes and long time scales. Atomistic simulations provide the required temperature dependent input quantities for the LLB equation, such as the equilibrium magnetization and the anisotropy and can be used to capture the detailed magnetization dynamics. The multiscale approach makes it possible to overcome the computational limitations of atomistic models in dealing with large systems, such as a recording track, while incorporating the basic physics of the HAMR process. We investigate the magnetization dynamics of a single FePt grain as a function of the properties of the temperature profile and applied field and test the LLB results against atomistic calculations. Our results prove the appropriateness and potential of the approach proposed here where the granular model is able to reproduce the atomistic simulations and capture the main properties of a HAMR medium.

DOI: [10.1103/PhysRevB.102.174419](https://doi.org/10.1103/PhysRevB.102.174419)

I. INTRODUCTION

The continuous increase in the virtual data generated by computers and mobile devices is pushing the limit of the current storage technology and alternatives are required. Current hard disk drives are able to reach areal storage densities up to about 1 Tbin^{-2} [1,2] with perpendicular magnetic recording (PMR) technology but face limitations to increase it beyond this point due to the so-called “magnetic recording trilemma” [3]: to further increase the areal storage density of recording media, smaller grains are needed; these grains need to have a high magnetic anisotropy [4] to be thermally stable; to write these high anisotropy grains, large head fields are required and these cannot be provided by a conventional write head. Heat assisted magnetic recording (HAMR) [1,5–7] represents the most promising alternative to conventional magnetic recording. HAMR technology exploits the fact that the magnetic anisotropy of a ferromagnetic material decreases with temperature as this approaches the Curie point (T_c). By heating the magnetic layer with a short and intense laser pulse to temperatures around T_c , the data can be written using a weaker magnetic field without affecting the data stability. The temperature assist makes possible the use of grains with larger magnetic anisotropy, therefore allowing for smaller grain diameters. These improvements have made it possible to obtain

storage densities of 1.4 Tbin^{-2} , as recently demonstrated by Seagate [7–11].

Despite HAMR being proposed and investigated for around 15 years, a complete understanding of the functioning of these devices necessary for the introduction into the market is lacking [2,12–16]. Moreover, engineering the medium by combining ferromagnets with different properties [4,17] and improving the head design can yield further increase in the storage density without compromising the reliability of the device [18]. In order for HAMR to be reliable, it is necessary that grains adjacent to the targeted region are not affected during the writing process. This could cause the undesired writing of such grains yielding large noise in the read back signal and thus degraded performances [5,19]. We aim to investigate on a theoretical and computational level the effects of temperature profile and thermal gradient on the magnetization dynamics and writing process of a realistic HAMR medium to be able to suggest improved design of the magnetic stack and writing head. We utilize a multiscale model of a granular HAMR medium where an atomistic spin model is combined with a macrospin (granular) approach. The atomistic approach is primarily employed to parametrize the main magnetic properties of the magnetic materials, such as magnetization, magnetic anisotropy, exchange coupling, and damping constant. This information is then used as input into the macroscopic spin (granular) model to investigate the magnetization dynamics in HAMR. The detailed mechanism of the magnetization reversal is also simulated by means of an atomistic spin model, although such a study is limited

*andrea.m@msu.ac.th

†jessada.c@msu.ac.th

to relatively small regions due to the heavy computational requirements. The comparison between the results obtained with the atomistic approach and the granular model allows us to validate our multiscale approach and provide extremely useful insights about the HAMR dynamics.

II. MODEL

A. Atomistic model

In the atomistic spin model one assumes that the magnetic moment can be localized on each atom, an approximation that works for the magnetic materials of interest in this work. Here the atomistic simulations are performed using the freely distributed software package VAMPIRE [20], where the interactions contributing to the internal energy are given by the following extended Heisenberg Hamiltonian [21]:

$$\mathcal{H} = - \sum_{i<j} J_{ij} \vec{S}_i \cdot \vec{S}_j - \sum_i k_u^i (\vec{S}_i \cdot \hat{e})^2 - \mu_0 \sum_i \mu_s^i \vec{S}_i \cdot \vec{H}_{\text{app}}. \quad (1)$$

J_{ij} is the exchange coupling constant for the interaction between the spins on site i (\vec{S}_i) and j (\vec{S}_j), k_u^i is the onsite uniaxial energy constant on site i along the easy axis \hat{e} , μ_s^i is the atomic spin moment on the atomic site i in units of μ_B , μ_0 is the permeability constant, and \vec{H}_{app} is the external applied field. The first term on the right hand side (RHS) of Eq. (1) represents the exchange coupling, the second the magnetic anisotropy energy, and the third the interaction with an external magnetic field. The dynamics of each individual spin is obtained by integrating the Landau-Lifshitz-Gilbert (LLG) equation of motion [21]:

$$\frac{\partial \vec{S}_i}{\partial t} = - \frac{\gamma}{1 + \lambda^2} [\vec{S}_i \times \vec{H}_{\text{eff}}^i + \lambda \vec{S}_i \times (\vec{S}_i \times \vec{H}_{\text{eff}}^i)]. \quad (2)$$

$\gamma = 1.761 \times 10^{11} \text{ T}^{-1} \text{ s}^{-1}$ is the electron gyromagnetic ratio, λ controls the damping and represents the coupling of spins to a heat bath through which energy can be transferred into and out of the spin system. \vec{H}_{eff}^i is the effective field acting on each spin obtained by differentiating the Hamiltonian [Eq. (1)] with respect to the atomic spin moment and accounts for the interactions within the system. Finite temperature effects are included under the assumption that the thermal fluctuations are noncorrelated and hence can be described by a white noise term. This is expressed as a Gaussian distribution in three dimensions whose first and second statistical moments of the distribution are:

$$\langle \xi_{i\alpha}(t) \rangle = 0, \quad (3)$$

$$\langle \xi_{ia}(t) \xi_{jb}(t') \rangle = \frac{2\lambda k_B T}{\mu_s \gamma} \delta_{ij} \delta_{ab} \delta(t - t'), \quad (4)$$

where i, j label spins on the respective sites, $a, b = x, y, z$ are the vector component of $\vec{\xi}$ in Cartesian coordinates, t, t' are the time at which the Gaussian fluctuations are evaluated, T is the temperature, δ_{ij} and δ_{ab} are Kronecker delta, and $\delta(t - t')$ is the delta function. Equation (3) represents the average of the random field, while Eq. (4) gives the variance of the field, which is a measure of the strength of its fluctuations. The

thermal contribution can be added to \vec{H}_{eff}^i :

$$\vec{H}_{\text{eff}}^i = - \frac{1}{\mu_s^i} \frac{\partial \mathcal{H}}{\partial \vec{S}_i} + \vec{H}_{\text{th}}^i. \quad (5)$$

B. Granular model

In our granular approach the magnetic medium is comprised of grains where each grain is treated as an individual macrospin of magnetization \vec{m} . Since HAMR devices involve the heating via a laser pulse of the magnetic medium close or up to T_c , a macrospin model based on the LLG dynamics is not the most appropriate choice, as this considers the length of the magnetization constant. Garanin [22] derived a macrospin equation of motion, the Landau-Lifshitz-Bloch (LLB) equation which accounts for the longitudinal relaxation of the magnetization. This is clearly important at elevated temperatures and therefore this is the formalism used in this work. Our macrospin simulations are based on the stochastic form of the LLB equation implemented following the work of Evans *et al.* [23]. The LLB equation of motion for each grain i reads:

$$\begin{aligned} \frac{\partial \vec{m}^i}{\partial t} = & \gamma (\vec{m}^i \times \vec{H}_{\text{eff}}^i) - \frac{\gamma \alpha_{\parallel}}{m^i} (\vec{m}^i \cdot \vec{H}_{\text{eff}}^i) \vec{m}^i \\ & + \frac{\gamma \alpha_{\perp}}{m^i} [\vec{m}^i \times (\vec{m}^i \times (\vec{H}_{\text{eff}}^i + \vec{\zeta}_{\perp}))] + \vec{\zeta}_{\text{ad}}. \end{aligned} \quad (6)$$

γ is the electron gyromagnetic ratio, \vec{m}^i is the reduced magnetization of grain i which represents the vector magnetization \vec{M}^i normalized by its equilibrium magnetization M_s , and m^i is the length of \vec{m}^i . The first and third terms on the RHS of Eq. (6) are the precessional and damping terms, respectively, for the transverse component of the magnetization, as in Eq. (2), while the second and fourth terms are introduced to account for the reduction of the longitudinal component of the magnetization with temperature. α_{\parallel} and α_{\perp} are the longitudinal and transverse damping parameters given by:

$$\alpha_{\parallel} = \frac{2}{3} \frac{T}{T_c} \lambda \quad \text{and} \quad \begin{cases} \alpha_{\perp} = \lambda (1 - \frac{T}{3T_c}), & \text{if } T \leq T_c \\ \alpha_{\perp} = \alpha_{\parallel} = \frac{2}{3} \frac{T}{T_c} \lambda, & \text{otherwise.} \end{cases} \quad (7)$$

In Eq. (7) λ is the atomistic damping parameter that couples the spin system with the thermal bath, the same entering the LLG equation for the atomistic approach [Eq. (2)]. ζ_{\perp} and ζ_{ad} are the terms that account for the thermal fluctuations in the limit that these can be treated as white noise. The thermal fields are described by Gaussian functions with zero average and variance (proportional to the strength of the fluctuations), analogously to the atomistic approach:

$$\begin{aligned} \langle \zeta_{ad}^i(t) \zeta_{ad}^j(t - t') \rangle &= \frac{2\gamma k_B T \alpha_{\parallel}}{M_s V} \delta_{ij} \delta_{ab} \delta(t) \\ \langle \zeta_{\perp}^i(t) \zeta_{\perp}^j(t - t') \rangle &= \frac{2k_B T (\alpha_{\perp} - \alpha_{\parallel})}{\gamma M_s V \alpha_{\perp}^2} \delta_{ij} \delta_{ab} \delta(t). \end{aligned} \quad (8)$$

\vec{H}_{eff}^i is the effective field that acts on each grain i :

$$\vec{H}_{\text{eff}} = \vec{H}_{\text{ani}} + \vec{H}_{\text{intragrain}} + \vec{H}_{\text{app}}. \quad (9)$$

The anisotropy field \vec{H}_{ani} is described following Garanin's approach [22]:

$$\vec{H}_{\text{ani}} = (m_x \hat{e}_x + m_y \hat{e}_y) / \tilde{\chi}_{\perp}, \quad (10)$$

where $\hat{e}_{x,y}$ is the unit vector aligned along the x, y directions, $m_{x,y}$ the reduced magnetization components along the x, y axis, and $\tilde{\chi}_{\perp}$ is the reduced perpendicular susceptibility, which gives the strength of the fluctuations of the components of the magnetization transverse to the easy axis and introduces the temperature dependence in \vec{H}_{ani} . This expression for the anisotropy field reduces to $2K/M_s$ at $T = 0$ K.

The intragrain exchange field $\vec{H}_{\text{intragrain}}$ accounts for the exchange coupling between the atoms within the grain i controlling the length of the magnetization at the atomistic level and has the form:

$$\vec{H}_{\text{intragrain}} = \begin{cases} \frac{1}{2\tilde{\chi}_{\parallel}} \left(1 - \frac{m^2}{m_e^2}\right) \vec{m}, & \text{if } T \leq T_c \\ -\frac{1}{\tilde{\chi}_{\parallel}} \left(1 + \frac{3}{5} \frac{T_c}{T - T_c} m^2\right) \vec{m}, & \text{otherwise} \end{cases}, \quad (11)$$

where m is the length of the grain reduced magnetization \vec{m} , $m_e(T)$ is the equilibrium magnetization, and $\tilde{\chi}_{\parallel}$ is the reduced parallel component of the susceptibility. It is worth noting that the term "exchange" refers only to the atomistic origin of the longitudinal relaxation of the magnetization. $\tilde{\chi}_{\parallel}$ represents the magnetization fluctuations along the easy axis and depends on temperature, as $\tilde{\chi}_{\perp}$. \vec{H}_{app} represents the externally applied magnetic field used to reverse the direction of the magnetization.

Finally, we point out that we have not included the magnetostatic contribution in our study neither within the atomistic nor within the granular model as we are interested in high temperature dynamics of a single grain. In HAMR processes the temperature approaches T_c and the magnetization shrinks decreasing the magnetostatic contribution that is proportional to it. Moreover, in our study we will focus on single grains and thus we do not have the contribution from other grains within the magnetic film. For these reasons we have neglected magnetostatic contributions in this study.

C. HAMR dynamics

In this study we concentrate on isolated grains dynamics and the atomistic parametrization of the macrospin LLB equation. We consider a simple analog of the HAMR process in which an external field H_{max} is applied along the z direction to the region under the writing head. The laser pulse $T(t)$ is modelled as a temperature pulse with Gaussian profile in time $T(t)$ while it is uniform in space:

$$T(t) = T_a + [T_{\text{peak}} - T_a] F(t), \quad (12)$$

where

$$F(t) = \exp \left[- \left(\frac{t - 3t_{\text{pulse}}}{t_{\text{pulse}}} \right)^2 \right] \quad (13)$$

is a Gaussian in one dimension with standard deviation $\sqrt{2}t_{\text{pulse}}$ and hence the maximum temperature T_{peak} of the pulse is reached at $3t_{\text{pulse}}$. T_a is the ambient temperature at which the system is left when no pulse is applied, usually room temperature. We remark that the results presented in

TABLE I. Simulation parameters for the investigated systems.

	FePt	Unit
J_{ij}	6.81×10^{-21}	J link ⁻¹
k_u	2.63×10^{-22}	J atom ⁻¹
μ_s	3.63	μ_B
T_c	690	K
K_u	9.23	J m ⁻³
$\mu_0 M_s$	1.32	T
λ	0.10	

this work are aimed to prove the goodness of the proposed approach and that these represent initial findings on a simple system composed of a single grain of the granular layer. As such, here we neglect the spatial dependence of the heat pulse and include only its time dependence. More complex systems and dynamics are the object of further studies and are not discussed in this work.

III. RESULTS

A. Multiscale parametrization of granular medium model

We consider a HAMR medium whose magnetic layer is composed of a single layer of identical, noninteracting grains comprised of fully chemically ordered tetragonally distorted fcc (fct) L1-0 FePt, where Fe and Pt occupy distinct planes. In this phase FePt is characterized by a large magnetocrystalline anisotropy [2] directed along the long axis of the grain (z axis) that provides the required thermal stability to retain the data over 10 years and relatively low T_c around 700 K. Moreover, ordered L1-0 FePt exhibits long range exchange coupling and two-ion anisotropy energy, which represents an anisotropic exchange interaction [24–26]. We model FePt mapping the fct structure to a distorted sc crystal structure with lattice vectors in the $x, y,$ and z directions $a_{0,x} = a_{0,y} = 0.272$ nm, $a_{0,z} = 0.385$ nm. Mryasov *et al.* [24] showed that the Pt moments are entirely induced by the Fe and can be replaced by substitution and an enhanced Fe moment of $3.23 \mu_B$. This yields a saturation magnetization M_s of 1.1×10^6 JT⁻¹ m⁻³ as in bulk FePt [26]. Here we use a simplified version of the Hamiltonian of Ref. [24] in which atoms are assigned a uniaxial anisotropy energy with $k_u = 2.63 \times 10^{-22}$ J atom⁻¹ and isotropic nearest-neighbors exchange coupling $J_{ij} = 6.81 \cdot 10^{-21}$ J link⁻¹. We assume $\lambda = 0.1$ for FePt in our study, a value accepted normally for compounds including heavy elements such as Pt and in agreement with the value reported in Ref. [27] obtained using an optical FMR technique on granular FePt. In our work we simulate single hexagonal FePt grains, both atomistically and by using a macrospin LLB model, whose material parameters are summarized in Table I.

We determine the temperature dependent equilibrium magnetization and susceptibility components of a single hexagonal FePt grain by performing time evolution of the magnetization and by averaging over 100 repetitions by means of atomistic calculations. We integrate the spin system for 100 000 steps with an integration step $dt = 1$ fs. The initial 50 000 steps are required to ensure that the spin system reaches thermal equilibrium and are therefore discarded.

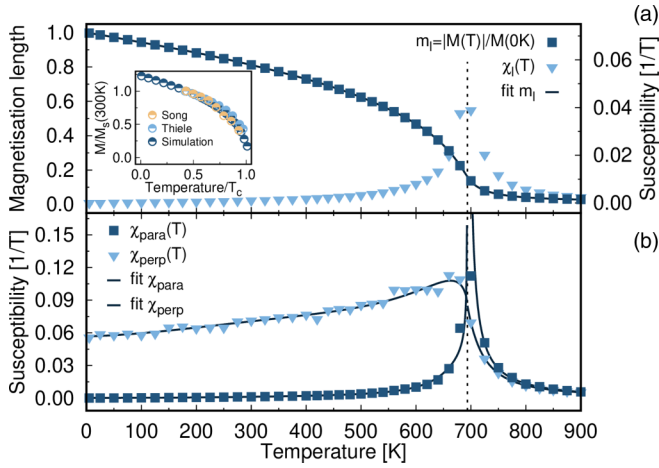


FIG. 1. Temperature dependence of (a) reduced magnetization length $m = |\vec{M}|/M(0 \text{ K})$ and reduced longitudinal susceptibility $\tilde{\chi}_l$, (b) reduced parallel and perpendicular susceptibility $\tilde{\chi}_{\parallel}$ and $\tilde{\chi}_{\perp}$, respectively, for a single $5 \times 5 \times 10 \text{ nm}^3$ FePt grain. Black continuous lines are fit to the data according to Eqs. (14) and (16). The comparison between calculated (dark blue) and measured (light blue from Thiele [28], yellow from Song [29]) magnetization temperature dependence normalized by the saturation value at 300 K is presented in the inset. Temperatures are normalized by the respective system Curie temperature T_c .

Only data corresponding to integration steps from 50 000 to 100 000 contribute to the presented results. Such an approach ensures good convergence. Classical spin dynamics yields a critical exponent of the magnetization as function of T_c around 0.3, a value close to what we obtain by fitting our simulations results assuming a bulk behavior. Experimentally, the magnetization shows a flatter trend at low temperature and a more critical behavior close to T_c . We compare our calculated magnetization temperature dependence by means of atomistic simulations with the experimental results obtained by Thiele *et al.* [28] and Song and collaborators [29], presented as inset in Fig. 1. Despite different values of M_s and T_c for each system, we do not observe significant differences between simulations and experiments when we normalize the data with respect to $M(300 \text{ K})$ and T_c in the temperature range of interest. We can expect small differences in the low temperature behavior of the magnetization between simulations and experiments. However, we believe our approach does not affect the accuracy of the results as here we focus on temperatures larger than 300 K. We note that this agreement is obtained without applying a temperature rescaling [30] which maps classical spin simulations onto the experimental behavior in the cases where quantum statistics dominate at low temperatures. This differs from assumptions in other works [31].

The granular LLB model requires the temperature dependence of the magnetization and that of the perpendicular and parallel susceptibilities as input parameters. We obtain these quantities by performing atomistic simulations and fitting the data, as shown in Fig. 1 for a $5 \times 5 \times 10 \text{ nm}^3$ FePt grain. The temperature dependent magnetization length $m(T) = M(T)/M(0 \text{ K})$ is fitted using a polynomial expression in $(T - T_c)/T_c$, as discussed by Kazantseva

TABLE II. Fitting parameters for m and $1/\tilde{\chi}_{\parallel,\perp}$, where a_i (b_i) are the coefficients for $T < T_c$ ($T \gtrsim T_c$).

	m	$1/\tilde{\chi}_{\parallel}$ [T]	$1/\tilde{\chi}_{\perp}$ [T]
a_0	0.1635	0.0	12.13
a_1	4.372	689.20	79.12
a_2	-22.90	-1460.0	-118.4
a_3	96.64	14178	121.4
a_4	-263.8	-30716	-47.47
a_5	446.5	25076	0.0
a_6	-450.6	0.0	0.0
a_7	247.6	0.0	0.0
a_8	-56.90	0.0	0.0
a_9	-0.0	0.0	0.0
$a_{1/2}$	-0.09447	22.131	-29.19
b_0		0.0	11.71
b_1	141.6	427.26	268.5
b_2	-145.9	142.34	1778.0
b_3		1842.5	-2794.0
b_4		-1762.5	1369.0

et al. [32]:

$$m(T) = \begin{cases} \sum_{i=0}^9 A_i \left(\frac{T_c - T}{T_c}\right)^i + A_{1/2} \left(\frac{T_c - T}{T_c}\right)^{1/2}, & \text{if } T < T_c \\ \left[\sum_{i=1}^2 B_i \left(\frac{T - T_c}{T_c}\right)^i + A_0^{-1} \right]^{-1}, & \text{otherwise.} \end{cases} \quad (14)$$

This formulation of $m(T)$ allows us to reproduce the finite-size effects captured by the atomistic spin dynamics simulations, see Fig. 1. The susceptibility expresses the strength of the fluctuations of the magnetization and, according to the spin fluctuation model, the components of the susceptibility can be obtained by the fluctuations of the same magnetization components as follows [33]:

$$\tilde{\chi}_{\alpha} = \frac{\mu_s N}{k_B T} (\langle m_{\alpha}^2 \rangle - \langle m_{\alpha} \rangle^2). \quad (15)$$

Here $\langle m_{\alpha} \rangle$ is the ensemble average of the reduced magnetization component $\alpha = x, y, z, l$, N is the number of spins in the system with magnetic moment μ_s , $k_B = 1.381 \times 10^{-23} \text{ J K}^{-1}$ is the Boltzmann constant, and T the temperature. l is the length of the magnetization, whereas x, y, z are the spacial components of the magnetization. $\tilde{\chi}_{\parallel}$ refers to the magnetization component along the easy-axis direction, which is z for our system, whereas $\tilde{\chi}_{\perp}$ describes the fluctuations of the magnetization in the plane perpendicular to the easy axis. For $\tilde{\chi}_{\parallel}$ and $\tilde{\chi}_{\perp}$ fitting functions we use a similar approach to Ellis [33]:

$$\frac{1}{\tilde{\chi}_{\parallel,\perp}} = \begin{cases} \sum_{i=0}^9 C_i \left(\frac{T_c - T}{T_c}\right)^i + C_{1/2} \left(\frac{T_c - T}{T_c}\right)^{1/2}, & \text{if } T < T_c \\ \sum_{i=0}^4 D_i \left(\frac{T - T_c}{T_c}\right)^i, & \text{otherwise,} \end{cases} \quad (16)$$

where C_i and D_i and T_c are fitting parameters. Once all these parameters are determined, the granular model is fully parametrized regarding the material properties. The list of the fitting parameters used to plot m and $1/\tilde{\chi}_{\parallel,\perp}$ in Fig. 1 is presented in Table II.

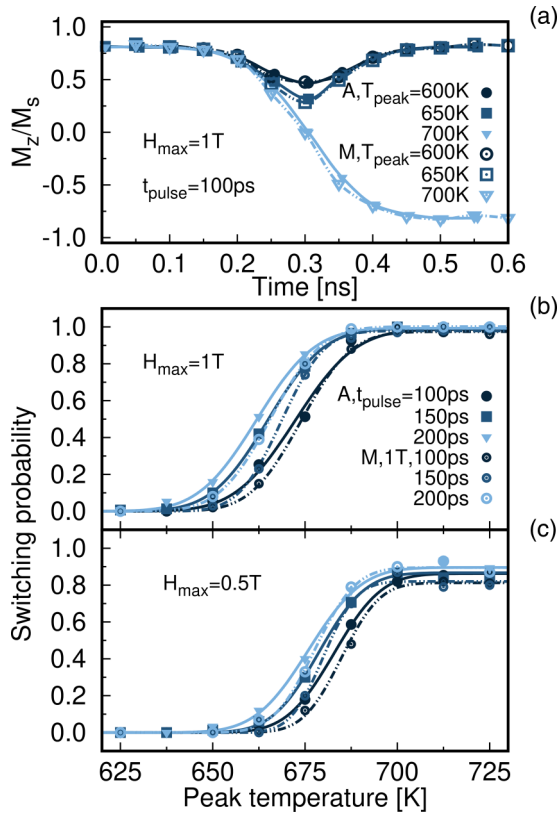


FIG. 2. (a) Time evolution of the z component of the magnetization (M_z/M_s) of a $5 \times 5 \times 10 \text{ nm}^3$ hexagonal grain of FePt subjected to an external field of 1 T and a temperature pulse $t_{\text{pulse}} = 100 \text{ ps}$ as a function of temperature. Comparison of atomistic (solid lines and filled symbols) and LLB (dotted lines and empty symbols) switching probabilities for $H_{\text{max}} = 1 \text{ T}$ (b) and 0.5 T (c) as a function of peak temperature for the same system.

B. Simulations of HAMR dynamics

We simulate the magnetization dynamics of a single $5 \times 5 \times 10 \text{ nm}^3$ FePt grain varying the peak temperature T_{peak} , length of the temperature pulse t_{pulse} , and values of the magnitude of the applied field $H_{\text{max}} = 0.5$ and 1 T, repeating each simulation 100 times to ensure a large enough statistical ensemble. For these simulations we use a smaller integration step of 0.1 fs in atomistic calculations to ensure the convergence of the results. The LLB equation is integrated using a 1 fs integration step. Differently from the atomistic calculations, we simulate the whole 100 grains in one single calculation with the granular model. Moreover, these calculations are about 15 times faster than the respective single grain atomistic simulations. On computing clusters batch parallel simulations can usually be performed. In our case this makes LLB simulations of 100 grains around 100 times faster than atomistic calculations. Figure 2(a) shows the time evolution of the z component and length of the magnetization subjected to a temperature pulse with $t_{\text{pulse}} = 100 \text{ ps}$ and different T_{peak} in an external field H_{max} of 1.0 T. For comparison, both atomistic and granular model calculations are shown. After the temperature pulse reaches the maximum, where the magnetization of the grain shrinks as $T_{\text{peak}} \sim T_c$, and the temperature decreases, the external field can reverse the magnetization. The

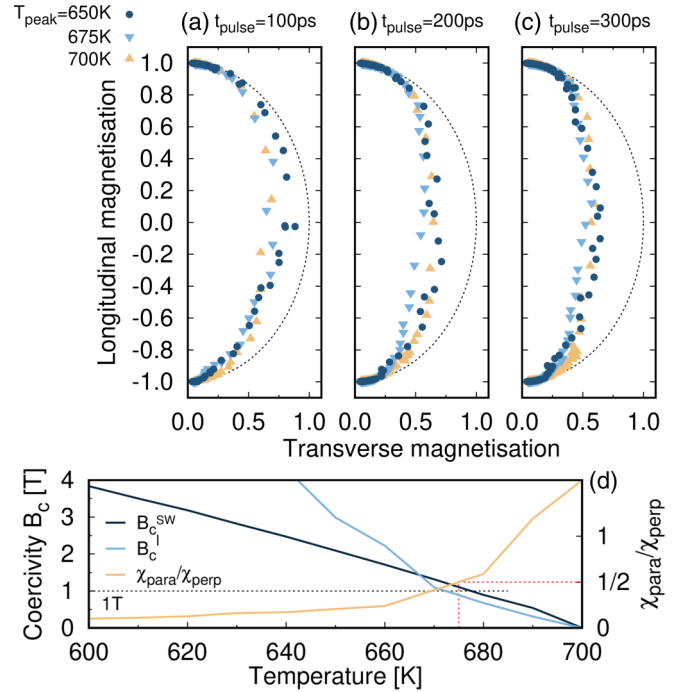


FIG. 3. Plot of the average longitudinal magnetization versus the transverse magnetization of a $5 \times 5 \times 10 \text{ nm}^3$ hexagonal grain of FePt for 100 (a), 200 (b), and 300 ps (c) pulse times and for heat pulses reaching peak temperatures of 650, 675, and 700 K under the application of an external field $H_{\text{app}} = 1 \text{ T}$ calculated over the successful switching events only of the 100 individual simulations. Dashed black lines show the circular reversal trajectory characteristic of a precessional dynamics. (d) Temperature dependence of coercivity for Stoner-Wohlfarth B_c^{SW} and linear B_c^{l} reversal mechanism (left axis) and susceptibility ratio $\tilde{\chi}_{\parallel}/\tilde{\chi}_{\perp}$ (right axis) for the same FePt grains. Red dashed line marks the transition temperature for linear reversal following the work in Ref. [32]; black dashed line marks the coercive field of 1 T.

effect of peak temperature is further studied by computing the switching probability as a function of peak temperature for different pulse duration. Results for applied field of 1, 0.5 T are shown in Figs. 2(b) and 2(c). The application of a weaker H_{max} cannot succeed in switching the magnetization due to the large thermal gradient of the pulse, which does not allow the individual spins within the grain to follow the field throughout the cooling process. The good agreement between the magnetization dynamics obtained by performing atomistic simulations and by using the granular model is proof that the latter incorporates the underlying thermal physics of the HAMR mechanism.

Further, we investigate the mechanism via which the magnetization of a grain reverses during the writing process in HAMR systems. We extract the average magnetization along the easy axis and perpendicular to it normalized by the average magnetization length to account for the change in the length as the temperature changes. The former, longitudinal magnetization, is $(M_z/M_s)/(\sum_i M_i/N)$ and the latter, transverse magnetization, is defined as $\sqrt{(M_x/M_s)^2 + (M_y/M_s)^2}/(\sum_i M_i/N)$. The average runs over only the successful switching events of the 100 simulations discussed above. This is shown in Fig. 3 for different pulse lengths and peak temperatures with

an applied field of 1.0 T for atomistic simulations. Results for LLB simulations are not presented for the sake of clarity as they would overlap. The dashed black line in panels (a), (b), and (c) depicts the circular reversal path characteristic of coherent precessional Stoner-Wohlfarth dynamics for a single domain particle, where a reduction in the longitudinal magnetization corresponds an increase of the transverse component. We can see that all the results start off following the circular trajectory until the transverse component reaches ~ 0.3 . As the magnetization dynamics evolves, the magnitude of the magnetization clearly decreases on approaching the hard direction: the main characteristic of a transition to elliptical and linear reversal. The transition between these different regimes corresponds to a temperature of 665 K. To understand the sudden change in the magnetization behavior at 665 K, we look at the ratio of susceptibilities $\tilde{\chi}_{\parallel}$ and $\tilde{\chi}_{\perp}$ for our system as a function of temperature, plotted as the yellow line in Fig. 3(d). Since $1/\tilde{\chi}_{\parallel}$ is proportional to the macroscopic longitudinal field of Eq. (11) and $1/\tilde{\chi}_{\perp}$ represents the anisotropy field, the ratio $\tilde{\chi}_{\parallel}/\tilde{\chi}_{\perp}$ defines the transitions between reversal mechanisms, as discussed by Kazantseva *et al.* [32]. Specifically, at low temperatures (for $\tilde{\chi}_{\parallel}/\tilde{\chi}_{\perp} < 1/3$) the circular (coherent) mechanism is dominant. At this point elliptical reversal, involving a shrinking of the magnetization along the hard direction, begins until $\tilde{\chi}_{\parallel}/\tilde{\chi}_{\perp} < 1/2$ at which point the transverse magnetization vanishes and linear reversal dominates. Here we make a comparison of the characteristic switching fields to indicate the likely reversal mechanism for a given temperature range. We extract the coercive field in the case of Stoner-Wohlfarth dynamics [$P_c^{SW} = 2K(T)/M_s(T)$], presented in Fig. 3(d). We also show the switching field for linear reversal following Ref. [32]. The expectation, according to a simple transition from circular to elliptical and linear reversal suggests that at the highest temperature of 700 K reversal should be completely linear. However, as shown in Figs. 3(a)–3(c) the reversal path we observe differs from the linear dynamics since the transverse component remains finite. We suggest that this is due to the timescale of the processes. According to Kazantseva *et al.* [32] the characteristic timescale of reversal is strongly field dependent and in the temperature range of interest at 1 T can be as much as many tens of picoseconds. As a result it is possible that at the rates of increase of temperature studied here the linear reversal mechanism is inaccessible. This further suggests a strong dependence of the reversal mechanism on the properties of the temperature pulse, such as duration and rate of increase. Therefore deeper analysis and investigations are required and will be the object of further study.

To better characterize the HAMR dynamics of our FePt grains, we register whether the grain magnetization reverses and count one if the grain switches, zero otherwise. By doing this, we build the switching probability of our system. We present in Figs. 2(b) and 2(c) the switching probability as a function of peak temperature T_{peak} comparing atomistic and LLB simulations for $H_{\text{max}} = 1.0$ T and $H_{\text{max}} = 0.5$ T, respectively. Small differences can be observed when comparing the switching probabilities calculated using the two approaches. Consider first the case of an applied field of 1T shown in Fig. 2. It can be seen that there is a small but systematic difference between the atomistic and macrospin

model predictions with a shift of a few degrees between the respective probability curves. We first observe that the range of temperatures we are considering is within 80 K of T_c , a critical regime for analytic approaches describing temperature dependent quantities. The LLB formalism was developed for bulk systems and does not exhibit the reduced criticality of the finite size atomistic model simulations. Empirically, numerical parametrization via Eqs. (14) and (16) is the simplest phenomenological approach to introduce finite size effects into the LLB formalism. The small differences between the atomistic and macrospin model predictions suggest that the numerical parametrization is a reasonable approach.

By exploiting the fact that each switching simulation is an independent event, we can treat it as a random variable and as such it is described by a normal distribution. The probability that the switching occurs is given by the cumulative distribution function. By fitting the switching probability as a function of peak temperature with the cumulative distribution function of a random variable we can extract the relevant parameters, such as the mean value μ and the width of the distribution σ . We express the cumulative distribution function following the discussion presented in Ref. [34]:

$$\Phi(\mu, \sigma, p_{\text{max}}) = \frac{1}{2} \left[1 + \operatorname{erf} \left(\frac{x - \mu}{\sqrt{2}\sigma} \right) \right] p_{\text{max}}, \quad (17)$$

where $\operatorname{erf}(x)$ is the error function and p_{max} is the average maximum achievable switching probability. σ gives the steepness of the cumulative function and is a measure of the jitter noise, a parameter indicative of the maximum areal density achievable by the medium as it relates to the bit transitions. $\sigma \sim 1/(dP(T)/dT)$ and therefore steeper switching probability as a function of temperature produce smaller jitter noise and are desirable. In addition, we can see from our results that $dP(T)/dT$ decreases with the magnitude of the applied field, in agreement with results presented in Ref. [35], because the temperature window available to reverse the grain magnetization reduces for a smaller applied field H_{max} . The maximum probability p_{max} depends on the applied field via the temperature gradient of the switching field, hence higher H_{max} yields larger p_{max} . Because the total noise depends on both the field gradient and switching probability gradient with respect to temperature, and these behave in opposite ways, a tradeoff is necessary to optimize HAMR media. From the switching probability one can access the bit error rate (BER), as discussed by Vogler *et al.* [36]. However, because of the low p_{max} reached by the FePt system and keeping into consideration that the results shown here are for a system composed of uncoupled grains and a simple writing process where heat and field are applied uniformly to each grain is used, we do not compute the BER. We combine the temperature and time dependence of the switching probability in phase plots showing the switching probability (color) as a function of the peak temperature T_{peak} and pulse time t_{pulse} for $H_{\text{max}} = 0.5$, 1.0 T, with steps of 12.5 K and 50 ps, respectively. We are able to perform these simulations by means of both granular model and atomistic calculations because the system is composed of an isolated single grain and consequently by only a few thousand atoms. Figure 4 shows the obtained phase plots for $H_{\text{max}} = 0.5$ T [4(a) and 4(c)] and $H_{\text{max}} = 1.0$ T [4(b) and

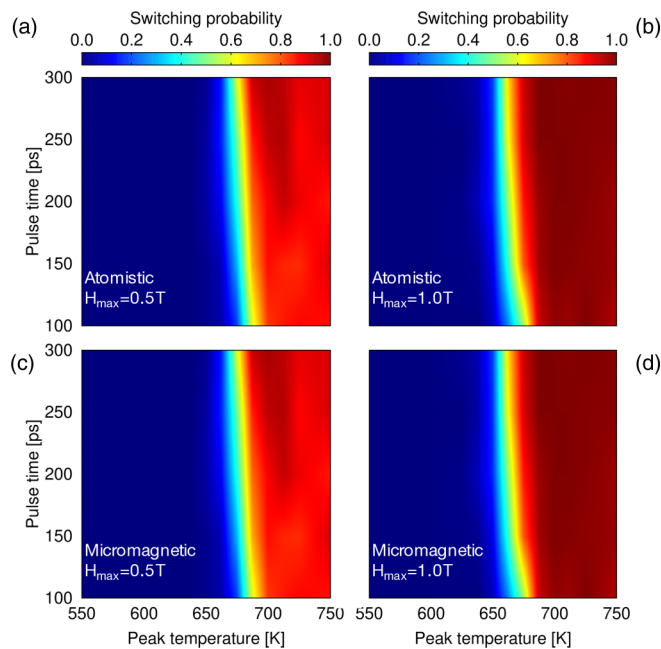


FIG. 4. Plot of the switching probability (color) for a single $5 \times 5 \times 10 \text{ nm}^3$ hexagonal grain of FePt as a function of pulse length t_{pulse} and peak temperature T_{peak} for $H_{\text{app}} = 0.5$ T (left) and $H_{\text{app}} = 1.0$ T (right) comparing atomistic (top) and LLB (bottom) simulations. T_{peak} and t_{pulse} are varied with steps of 12.5 K and 50 ps, respectively.

4(d)] comparing atomistic (top) and LLB (bottom) simulations. The two different methods yield very similar results, as mentioned above, and hence we can use the LLB dynamics to perform more extensive calculations. From these phase plots we can observe how shorter time pulses require higher peak temperatures to achieve a successful magnetization reversal for a given external field. Similarly, stronger H_{\max} needs to be applied for short t_{pulse} at a fixed temperature, which suggests the necessity for a tradeoff between H_{\max} , t_{pulse} , and T_{peak} . A feature emerging from our results is that the magnetization of a single grain of a HAMR granular medium can be reversed with probability larger than 0.9 only when the peak temperature is above T_c and for strong applied fields.

IV. CONCLUSIONS

In summary, we have presented a multiscale approach that combines atomistic and LLB-based macrospin simulations to model and describe HAMR media and their dynamics. The multiscale approach on one side exploits the high detail achievable throughout atomistic calculations and on the other uses this to provide the input parameters necessary to model LLB dynamics. This method makes it possible to overcome the computational limitations in dealing with large systems of atomistic simulations while retaining the high accuracy in the results. Our initial simulations prove the appropriateness and potential of the approach here proposed where the granular model is able to reproduce the atomistic simulations and main properties of a HAMR medium can be modelled. We show that careful atomistic parametrization of the LLB equation is important in order to take into account the effects of finite grain size. As an initial study we have modelled the simple case of a single isolated FePt grain subjected to spatially uniform field and temperature pulses. The grain size of 5 nm is smaller than current designs and represents an investigation of future HAMR media. Only switching probabilities obtained under the assumption of a 1 T field, the maximum likely for inductive technology, show good performances. Therefore, alternatives such as magnetic layers made of exchange coupled composite (ECC) materials [4,37,38] need to be pursued to make HAMR a viable technology. In addition, the magnetization dynamics exhibits a mixture of precessional and linear character, differently from what is commonly assumed for HAMR processes. Our results suggest a strong dependence of the reversal mechanism on the properties of the temperature pulse. These aspects are crucial to improve HAMR technology and will be the subject of future work.

ACKNOWLEDGMENTS

J.C. would like to acknowledge the financial support from Maharakham University. The authors gratefully acknowledge the funding from Transforming Systems through Partnership Programme of the Royal Academy of Engineering under Grant No. TSP1285 and Seagate Technology (Thailand). Financial support of the Advanced Storage Research consortium is gratefully acknowledged. The simulations were undertaken on the VIKING cluster, which is a high-performance compute facility provided by the University of York.

- [1] R. E. Rottmayer, S. Batra, D. Buechel, W. A. Challener, J. Hohlfield, Y. Kubota, L. Li, B. Lu, C. Mihalcea, K. Mountfield, K. Pelhos, C. Peng, T. Rausch, M. A. Seigler, D. Weller, and X. M. Yang, Heat-assisted magnetic recording, *IEEE Trans. Magn.* **42**, 2417 (2006).
- [2] D. Weller, G. Parker, O. Mosendz, A. Lyberatos, D. Mitin, N. Y. Safonova, and M. Albrecht, Review Article: FePt heat assisted magnetic recording media, *J. Vac. Sci. Technol. B* **34**, 060801 (2016).
- [3] R. F. L. Evans, R. W. Chantrell, U. Nowak, A. Lyberatos, and H.-J. Richter, Thermally induced error: Density limit for magnetic data storage, *Appl. Phys. Lett.* **100**, 102402 (2012).
- [4] P. Chureemart, R. F. L. Evans, R. W. Chantrell, P.-W. Huang, K. Wang, G. Ju, and J. Chureemart, Hybrid Design For Advanced Magnetic Recording Media: Combining Exchange-Coupled Composite Media With Coupled Granular Continuous Media, *Phys. Rev. Appl.* **8**, 024016 (2017).
- [5] D. Weller, G. Parker, O. Mosendz, E. Champion, B. Stipe, X. Wang, T. Klemmer, G. Ju, and A. Ajan, A HAMR media technology roadmap to an areal density of 4 Tb/in², *IEEE Trans. Magn.* **50**, 1 (2014).
- [6] M. Kryder, E. Gage, T. McDaniel, W. Challener, R. Rottmayer, G. Ju, Y.-T. Hsia, and M. Erden, Heat assisted magnetic recording, *Proc. IEEE* **96**, 1810 (2008).

- [7] C. Rea, P. Subedi, K. Gao, H. Zhou, P.-L. Lu, P. J. Czoschke, S. Hernandez, M. Ma, R. Lopusnik, Y. Peng *et al.*, Areal-density limits for heat-assisted magnetic recording and perpendicular magnetic recording, *IEEE Trans. Magn.* **52**, 1 (2016).
- [8] A. Q. Wu, Y. Kubota, T. Klemmer, T. Rausch, C. Peng, Y. Peng, D. Karns, X. Zhu, Y. Ding, E. K. C. Chang, Y. Zhao, H. Zhou, K. Gao, J. Thiele, M. Seigler, G. Ju, and E. Gage, HAMR areal density demonstration of 1+ Tbps on spinstand, *IEEE Trans. Magn.* **49**, 779 (2013).
- [9] G. Ju, Y. Peng, E. K. Chang, Y. Ding, A. Q. Wu, X. Zhu, Y. Kubota, T. J. Klemmer, H. Amini, L. Gao, Z. Fan, T. Rausch, P. Subedi, M. Ma, S. Kalarickal, C. J. Rea, D. V. Dimitrov, P. W. Huang, K. Wang, X. Chen, C. Peng, W. Chen, J. W. Dykes, M. A. Seigler, E. C. Gage, R. Chantrell, and J. U. Thiele, High density heat-assisted magnetic recording media and advanced characterization—progress and challenges, *IEEE Trans. Magn.* **53**, 1 (2017).
- [10] S. D. Granz, T. Ngo, T. Rausch, R. Brockie, R. Wood, G. Bertero, and E. C. Gage, Definition of an areal density metric for magnetic recording Systems, *IEEE Trans. Magn.* **53**, 1 (2017).
- [11] C. Rea, P. Czoschke, P. Krivosik, V. Sapozhnikov, S. Granz, J. Zhu, Y. Peng, J.-U. Thiele, G. Ju, and M. Seigler, High track pitch density for HAMR recording: 1M tpi, *IEEE Trans. Magn.* **55**, 1 (2019).
- [12] H. Richter and G. Parker, Temperature dependence of the anisotropy field of L10 FePt near the Curie temperature, *J. Appl. Phys.* **121**, 213902 (2017).
- [13] J. Waters, D. Kramer, T. J. Sluckin, and O. Hovorka, Resolving Anomalies in the Critical Exponents of FePt Using Finite-Size Scaling in Magnetic Fields, *Phys. Rev. Appl.* **11**, 024028 (2019).
- [14] M. Strungaru, S. Ruta, R. F. L. Evans, and R. W. Chantrell, Model of Magnetic Damping and Anisotropy at Elevated Temperatures: Application to Granular FePt Films, *Phys. Rev. Appl.* **14**, 014077 (2020).
- [15] S. Hernández, P.-L. Lu, S. Granz, P. Krivosik, P.-W. Huang, W. Eppler, T. Rausch, and E. Gage, Using ensemble waveform analysis to compare heat assisted magnetic recording characteristics of modeled and measured signals, *IEEE Trans. Magn.* **53**, 1 (2017).
- [16] Z. Liu, P.-W. Huang, G. Ju, and R. H. Victora, Thermal switching probability distribution of L10 FePt for heat assisted magnetic recording, *Appl. Phys. Lett.* **110**, 182405 (2017).
- [17] W. Daeng-am, P. Chureemart, R. W. Chantrell, and J. Chureemart, Granular micromagnetic model for perpendicular recording media: Quasi-static properties and media characterisation, *J. Phys. D* **52**, 425002 (2019).
- [18] Z. Liu, Y. Jiao, and R. Victora, Composite media for high density heat assisted magnetic recording, *Appl. Phys. Lett.* **108**, 232402 (2016).
- [19] J. G. Zhu and H. Li, Understanding signal and noise in heat assisted magnetic recording, *IEEE Trans. Magn.* **49**, 765 (2013).
- [20] Computer code VAMPIRE.
- [21] R. F. L. Evans, W. J. Fan, P. Chureemart, T. A. Ostler, M. O. A. Ellis, and R. W. Chantrell, Atomistic spin model simulations of magnetic nanomaterials, *J. Phys.: Condens. Matter* **26**, 103202 (2014).
- [22] D. A. Garanin, Fokker-planck and Landau-Lifshitz-Bloch equations for classical ferromagnets, *Phys. Rev. B* **55**, 3050 (1997).
- [23] R. F. L. Evans, D. Hinze, U. Atxitia, U. Nowak, R. W. Chantrell, and O. Chubykalo-Fesenko, Stochastic form of the Landau-Lifshitz-Bloch equation, *Phys. Rev. B* **85**, 014433 (2012).
- [24] O. N. Mryasov, U. Nowak, K. Y. Guslienko, and R. W. Chantrell, Temperature-dependent magnetic properties of FePt: effective spin Hamiltonian model, *Europhys. Lett.* **69**, 805 (2005).
- [25] N. Kazantseva, Dynamic response of the magnetization to picosecond heat pulses, Ph.D. thesis, University of York (2008).
- [26] M. O. Ellis and R. W. Chantrell, Switching times of nanoscale FePt: finite size effects on the linear reversal mechanism, *Appl. Phys. Lett.* **106**, 162407 (2015).
- [27] J. Becker, O. Mosendz, D. Weller, A. Kirilyuk, J. C. Maan, P. C. M. Christianen, T. Rasing, and A. Kimel, Laser induced spin precession in highly anisotropic granular L10 FePt, *Appl. Phys. Lett.* **104**, 152412 (2014).
- [28] J. U. Thiele, K. R. Coffey, M. F. Toney, J. A. Hedstrom, and A. J. Kellock, Temperature dependent magnetic properties of highly chemically ordered Fe_{55-x}Ni_xPt₄₅L1₀ films, *J. Appl. Phys.* **91**, 6595 (2002).
- [29] J. Song, J. Wang, D. Wei, Y. Takahashi, and K. Hono, Micromagnetic studies at finite temperature on FePt-C granular films, in *Proceedings of the 2017 IEEE International Magnetism Conference (INTERMAG), Dublin, Ireland* (IEEE, Piscataway, NJ, 2017).
- [30] R. F. L. Evans, U. Atxitia, and R. W. Chantrell, Quantitative simulation of temperature-dependent magnetization dynamics and equilibrium properties of elemental ferromagnets, *Phys. Rev. B* **91**, 144425 (2015).
- [31] Razvan-V. Ababei, M. O. A. Ellis, R. F. L. Evans, and R. W. Chantrell, Anomalous damping dependence of the switching time in Fe/FePt bilayer recording media, *Phys. Rev. B* **99**, 024427 (2019).
- [32] N. Kazantseva, D. Hinze, R. W. Chantrell, and U. Nowak, Linear and elliptical magnetization reversal close to the Curie temperature, *Europhys. Lett.* **86**, 27006 (2009).
- [33] M. Ellis, Simulations of magnetic reversal properties in granular recording media, Ph.D. thesis, University of York (2015).
- [34] O. Muthsam, C. Vogler, and D. Suess, Curie temperature modulated structure to improve the performance in heat-assisted magnetic recording, *J. Magn. Magn. Mater.* **474**, 442 (2018).
- [35] D. Suess, C. Vogler, C. Abert, F. Bruckner, R. Windl, L. Breth, and J. Fidler, Fundamental limits in heat-assisted magnetic recording and methods to overcome it with exchange spring structures, *J. Appl. Phys.* **117**, 163913 (2015).
- [36] C. Vogler, C. Abert, F. Bruckner, D. Suess, and D. Praetorius, Areal density optimizations for heat-assisted magnetic recording of high-density media, *J. Appl. Phys.* **119**, 223903 (2016).
- [37] R. H. Victora and X. Shen, Exchange coupled composite media, *Proc. IEEE* **96**, 1799 (2008).
- [38] D. Suess, J. Lee, J. Fidler, and T. Schrefl, Exchange-coupled perpendicular media, *J. Magn. Magn. Mater.* **321**, 545 (2009).